Journal of Power Sources 207 (2012) 111–119

Contents lists available at SciVerse ScienceDirect

Journal of Power Sources

journal homepage: www.elsevier.com/locate/jpowsour

Characteristic study on fuel cell/battery hybrid power system on a light electric vehicle

Jenn Jiang Hwang[a,*], Wei Ru Chang[b]

[a] Department of Greenergy, National University of Tainan, Tainan, Taiwan
[b] Department of Landscape Architecture, Fu Jen Catholic University, Taipei, Taiwan

ARTICLE INFO

Article history:
Received 5 January 2012
Received in revised form 1 February 2012
Accepted 2 February 2012
Available online 11 February 2012

Keywords:
Light electric vehicle
Hybrid power system
Proton exchange membrane fuel cell
Lithium-ion battery

ABSTRACT

A light electric vehicle (LEV) equipped a hybrid power system has been developed in the present work. The hybrid power system consisted of a proton exchange membrane (PEM) fuel cell and a lithium-ion battery. The former serves the major propulsion power, while the later takes some of the peak power requirement as well as allows regenerative braking. First, major components of the hybrid power system such as a fuel cell stack, a membrane humidifier, a lithium-ion battery pack, a microcontroller, a DC/DC converter, and hydrogen storage canisters (HSCs) are developed and verified. Special attention will be placed on the implementation of the stack-humidifier assembly and the hydrogen storage canister. Then, a breadboard test to assess the efficiency of the hybrid power system is provided. Subsequently, a driving test and demonstration of the hybrid LEV is carried out. Finally, the proportion of power from the fuel cell and the lithium-ion battery is analyzed under various driving conditions such as idle, starting, acceleration, and braking. Results of this work might help directing future studies on the hybrid power system in the most promising way.

1. Introduction

Security of energy supply, high oil prices, and growing emissions of greenhouse gases (GHGs) continue to pose unresolved challenges for the global economy and the climate of the planet [1–3]. The transport sector should be greatly responsible for these situations since current transportations primarily rely on the fossil-fuel-based internal combustion engines (ICEs). When the ICE is running on fossil fuels, it emits carbon dioxides and other exhaust gases, which lead to harmful environmental problems such as the greenhouse effect, acid rain and air pollution. To wean off fossil fuels in our world, it is necessary to develop alternative fuel vehicles those produce less harmful impacts to the environment than conventional ICE vehicles [4,5].

Many kinds of alternative fuel vehicles are continuously being developed for decades such as hybrid electric vehicles (HEVs), plug-in hybrid electric vehicles (PHEVs), battery electric vehicles (BEVs), fuel cell vehicles (FCVs), natural gas vehicles, clean diesel vehicles, and vehicles using blends of biodiesel and ethanol fuel or gasohol [6,7]. Among them, the pure electric vehicles BEVs and FCVs are most promised since they are free of emissions. The electricity for driving BEVs is stored in the on-board storage (battery), while the electricity for propelling FCVs is generated from the on-board generator (fuel cell engine). Both electric vehicles will provide a deep change in how people transport goods and themselves by allowing electricity to become the primary transportation energy instead of petroleum.

Basically, fuel cells and batteries are complementary vehicle technologies rather than competing with each other. Fuel cells enable longer-range large vehicles and fast fueling. Batteries are good for shorter-range urban vehicles and to capture and store energy from braking, making the vehicle more efficient. Actually, automakers have used both technologies to create a wider variety of vehicles that can reduce GHGs more than by using batteries or fuel cells alone. That is most fuel cell vehicles (e.g., Honda FCX Clarity and Toyota FCV-R) feature a fuel cell-battery drivetrain, where the battery can take some of the peak power needs, thereby reducing the size of the fuel cell, and allow regenerative braking [8].

The object of this work is to develop a fuel cell/battery hybrid power system that propels a light electric vehicle (LEV). First, the availability of key components of the hybrid power system, such as a fuel cell stack, a membrane humidifier, a lithium-ion battery pack, a microcontroller, a DC/DC converter, and hydrogen storage canisters (HSCs), were verified. Then, a breadboard test was conducted to evaluate the efficiency of the hybrid power system. Subsequently, a driving test and demonstration of the LEV equipped the hybrid power system was carried out. Finally, the hybridization level between the fuel cell and the lithium-ion battery of the LEV was examined on various driving conditions such as idle, starting, acceleration, and braking. The major contribution of this work would be to successfully integrate a fuel cell stack and a membrane humidifier into a compact unit that has the advantages in the

* Corresponding author. Tel.: +886 62600321; fax: +886 62602251.
E-mail address: azaijj@mail.nutn.edu.tw (J.J. Hwang).

0378-7753/$ – see front matter © 2012 Elsevier B.V. All rights reserved.
doi:10.1016/j.jpowsour.2012.02.008

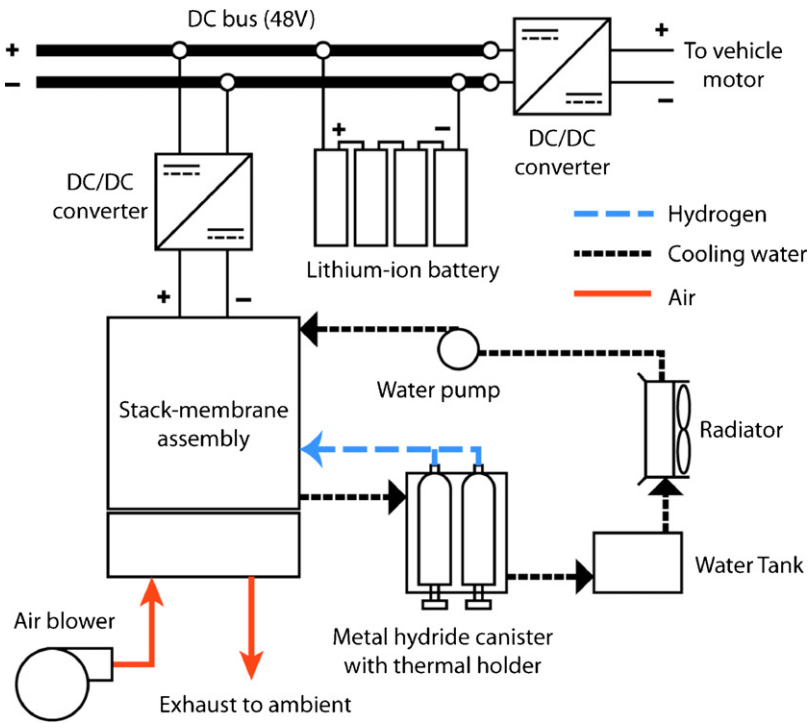

Fig. 1. Schematic drawing of the fuel cell/battery hybrid power system.

reduction of components and space saving. In addition, this work has thermally coupled the fuel cell stack and the metal hydride storage that recycles the thermal wastes from the fuel cell stack for desorption of hydrogen. Consequently, the present hybrid power system has a higher efficiency than the previous prototype [8]. The results obtained from this work feeding back for fundamental research efforts could steer future studies on the hybrid power system in the most promising direction [9–11].

2. Key component developments

The proton exchange membrane (PEM) fuel cell appears best suited for vehicular applications [8,12] and thus is employed in the present work. There has been much research into hydrogen fuel cell vehicles in the recent past such as optimal purification of fuel cell grade hydrogen [13], optimal operating points and automatic control [14], cold start ability in low temperature conditions [15], and many other operating characteristics [16,17]. Recently published simulation tools will assist researchers in the future as they continue to bring fuel cell technology to maturity [18–24]. Component degradation and durability is anticipated to be a critical issue for the practical use of fuel cells [25].

Fig. 1 shows a scheme of the fuel cell/battery hybrid power system for the light electric vehicle. The vehicle chassis together with the electric motor, and the transmission system used in the present work is Toyota AUTOBODY COMS, as shown in Fig. 2. The key

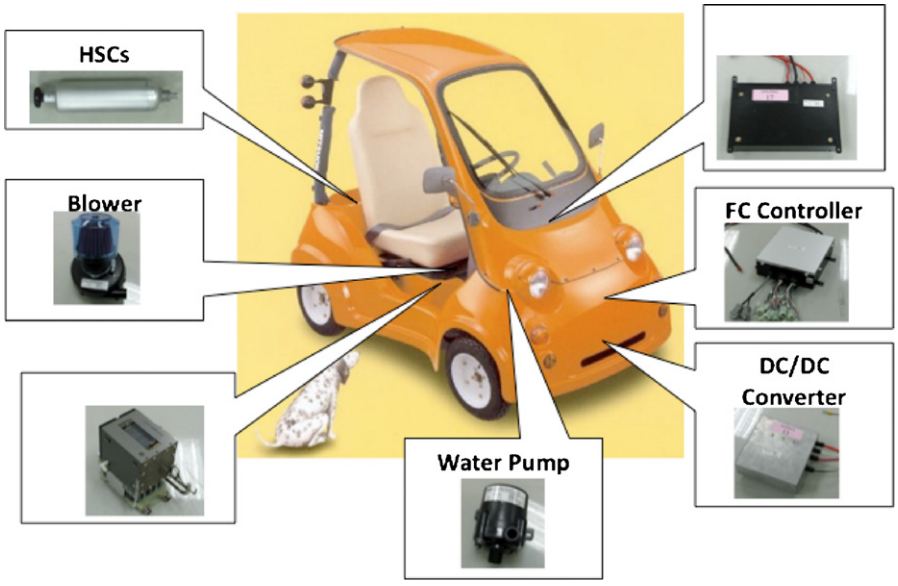

Fig. 2. Key components of the light electric vehicle.

Fig. 3. Stack-humidifier assemblies.

components of the hybrid power system indexed in the figure include a fuel cell stack, an air blower, a water pump, a lithium-ion battery pack, a fuel cell controller, a DC/DC converter, and hydrogen storage canisters (HSC) together with passive heating holders. Details of the development of the above key components are described below.

2.1. Stack-humidifier assembly

In order to reduce the redundant pipes and fitting and space saving, the PEM fuel cell stack and the membrane humidifier are integrated into a compact unit. As shown in Fig. 3, the stack-humidifier assembly has a fuel cell stack of 74 cells in series and a membrane-based humidifier (Table 1).

Before testing the polarization curve of the stack-humidifier assembly, it is important to identify the performance of the membrane humidifier. Fig. 4 shows the performance of the membrane humidifier. It is expressed as the airflow rate in relation to the pressure drop and the dew-point approach temperature. The dew-point approach temperature is defined as the dew-point difference between the cathode exhaust stream entering the humidifier and the humidified stream going to the stack. For example, if the cathode exhaust dew point entering the humidifier is 65 °C and the humidifier generates a cathode inlet dew point of 58 °C, it would have been sized for a 7 °C dew-point approach temperature. In the

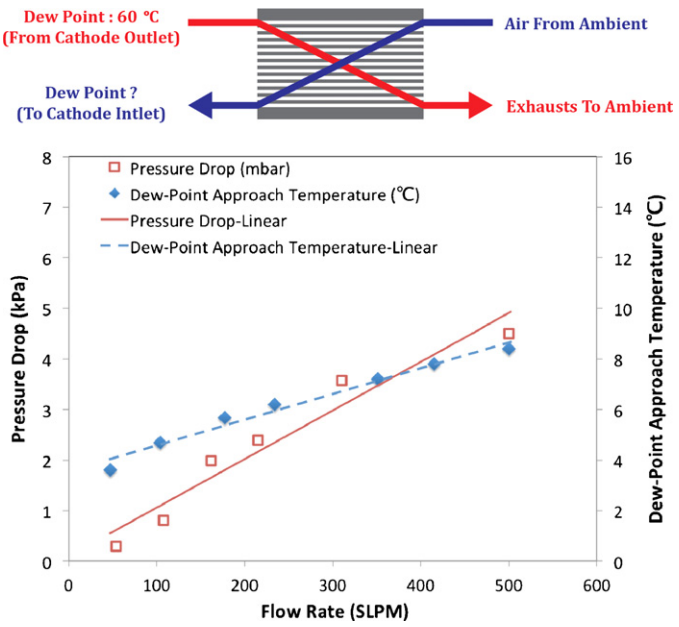

Fig. 4. Effect of flow rate on the difference of dew point of two flows between the cathode outlet and inlet. (For interpretation of references to color in the text, the reader is referred to the web version of this article.)

experiment, the primary flow (red arrow) simulates the cathode exhaust stream while the secondary flow (blue arrow) simulates the fresh air entering in the membrane humidifier. Both streams have the same flow rate. The dew point of the primary stream is controlled at 60 °C by passing the primary stream through a heated bubble humidifier. The fresh air entering the membrane humidifier has a temperature of 25 °C and a relative humidity of 40% (i.e., dew point about 10 °C). It is seen from Fig. 3 that the dew-point approach temperature is increased with increasing the flow rate. In the range of the airflow rate investigated, the dew-point approach temperature is less than 9 °C. Note also that the pressure drop across the membrane humidifier is increased with the airflow rate as well, meaning that the higher drag required more pumping power driving the cathode stream under higher power conditions.

Fig. 5 shows the performance of the stack-humidifier assembly under real operational conditions. Fresh air from the laboratory enters the stack-humidifier assembly with a temperature of 25 °C and a relative humidity of 40%. The air blower controls the stoichiometry of the cathode airflow at 2.5. It is seen from Fig. 4 that the present stack-humidifier assembly has a nominal power of 3.4 kW at 48VDC and a maximum power of 6.0 kW at the cut-off voltage (40 VDC). The above results are largely similar to those obtained for the stack alone on the commercial test standing, in which the humidity condition of the cathode inlet stream has been well controlled. This means that the present compact design in assembling the fuel

Table 1
Specification of the membrane humidifier.

Item	Value
Fuel cell rated power	6 kW
Rated flow	500 SLPM
Membrane material	Nafion® membrane
Rated continuous operating temperature	80 °C
Dew point approach temperature at rated flow, temperature and pressure	<8.5 °C
Pressure drop across the humidifier	<5 kPa
Maximum burst pressure	150 kPag
Power requirement	0 W

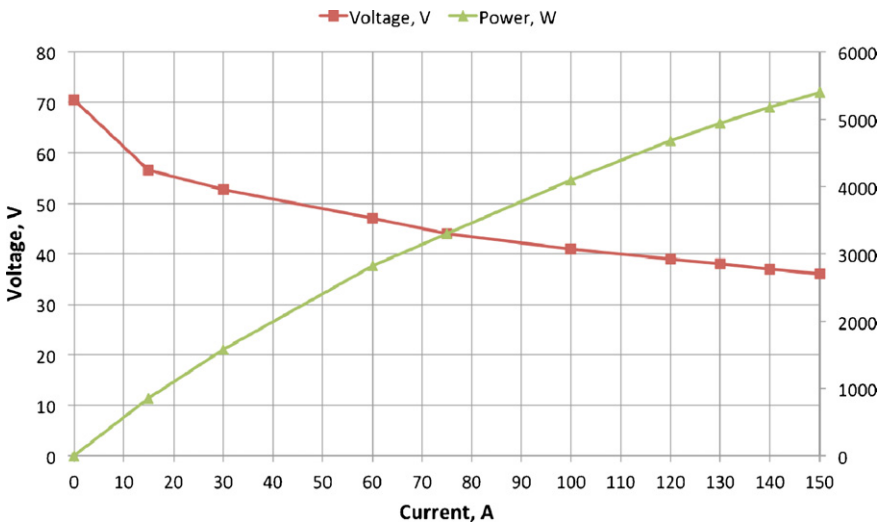

Fig. 5. Polarization curve of the stack-humidifier assembly.

cell stack and the membrane humidifier is proper, and thus has the benefits in reducing pipes and fittings as well as space saving.

2.2. Metal hydride canister

Storage of hydrogen in metal hydrides is attractive due to their high volumetric capacity. They have the potential for reversible on-board hydrogen storage for portable power and vehicular applications [26]. The metal hydrides release hydrogen at low temperatures (25–120 °C) and low pressures (1–10 atm), which is compatible for the operating conditions of a PEM fuel cell. Therefore, it is likely to use the waste heat dissipated by the PEM fuel cell stack (less than 80 °C) to stimulus the hydrogen release from the metal hydrides.

In the present design, the hydrogen is stored in an aluminum canister containing AB5 (LaNi5H6) alloy powders. The specification of the metal-hydride canister is given in Table 2. The internal structure of the canister has been designed for improvement of heat transfer inside the canister [27–29]. Fig. 6 shows the dynamics of hydrogen discharge from the metal hydrides. During the experiment, a water bath controlled the discharge temperature at 50 °C, while a mass flow controller (MFC) controlled the discharge flow rate at 8.2 SLPM. It is clearly seen from Fig. 6 that the pressure in the metal-hydride canister is gradually decreased during the hydrogen discharge process. The cut-off pressure is about 150 kPa, where the hydrogen discharge flow rate dropped abruptly. This means that the metal hydrides in the canister could last the hydrogen flow rate of 8.2 SLPM over 55 min. By subtracting the canister weight of discharged hydrogen from the refilled one, the amount of hydrogen discharged from the canister is about 45.8 g.

Table 2
Specifications of metal-hydride canister and canister holder.

	Characteristics	Specification
Canister	Hydrogen storage capacity	>45 gH2 per canister
	Canister material	Aluminum 6061-T6 alloy
	Canister dimension	Diameter: 76 mm; length: 365 mm
	Safety protection	Over pressure relief valve (580 psig)
	Metal hydride material	AB5 alloy
	Hydrogen purity requirement	>99.99%; O2, CO, S < 1 ppm
	Recommended charging condition	140 psig @ 10–20 °C
	Hydrogen discharge rate	a. >45 g/canister @ 7.5–8.2 slpm, 50 °C b. >39 g/canister @ 15–16 slpm, 50 °C
	Weight	4.4 ± 0.1 kg per canister
Holder	Weight	1.23 kg
	Dimension ($L \times W \times H$)	110 × 101 × 293 mm
	Heat transfer ability, kcal h^{-1} °C	11.24 @ 1.9 L min^{-1}

2.3. Thermal canister holder

Desorption of hydrogen from metal hydrides is endothermic, while the electrochemical reaction in fuel cells is exothermic. Hence, it is very conceivable to couple thermally the fuel cell with the metal hydride during the power extraction [30]. That is the stack coolant to extract the waste heat from the fuel cell stack is circulated through the metal hydrides to provide the heat required for desorption of hydrogen from the metal hydrides.

As shown in Fig. 7, the present work has designed a thermal holder to hold the metal-hydride canister [31]. The hot-water tubes coiled the shell surface of the holder (Fig. 7(a)). Additional insulation clothes covered the outside of the holder (Fig. 7(b)). The metal-hydride canister is then pushed into the thermal holder to connect the anode pipeline for hydrogen supply (Fig. 7(b))

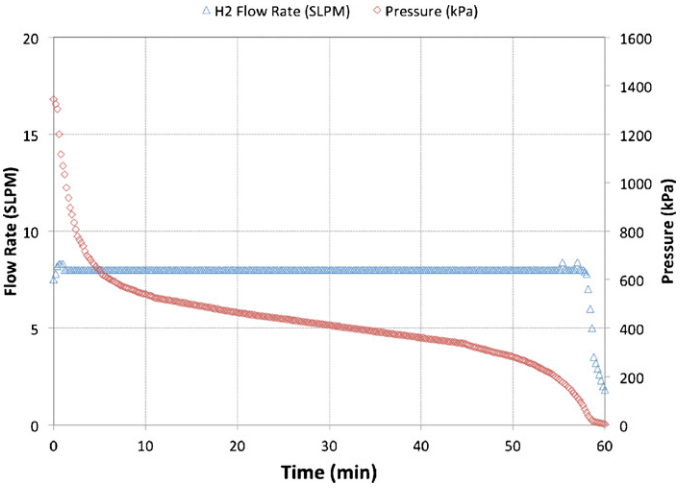

Fig. 6. Pressure histories of the metal hydride for discharging hydrogen at the constant flow rate of 8.2 SLPM.

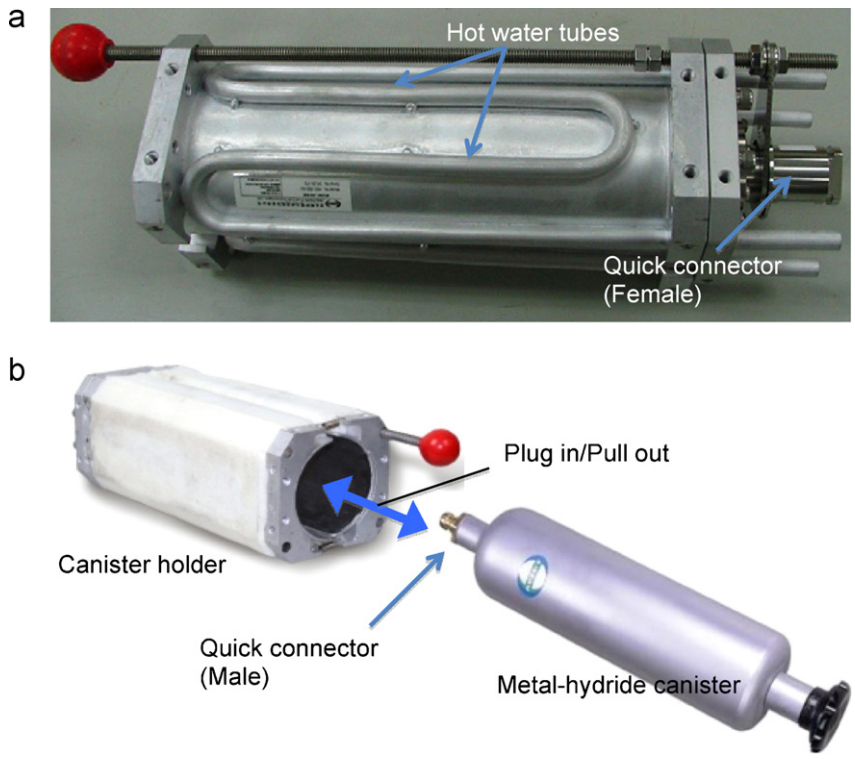

Fig. 7. (a) Photo of the canister holder, (b) assembly of metal-hydride canister and its holder.

When the hydrogen is discharged from the metal hydride canister, the metal hydrides inside the canister would reduce their temperature. Meanwhile, the hot water from the stack coolant outlet is circulated around the thermal holder that provides the thermal energy to the metal hydride to maintain their dynamics of hydrogen desorption.

The above design has the advantages in enhancing the system efficiency due to the recovery of thermal energy from the stack coolant and the reduction in the load on the radiator. According to the measurements, the canister thermal holder has a thermal capacity about 11.24 kcal h^{-1} K^{-1} at the water flow rate of 1.9 SLPM.

It is interested to note that the metal-hydride canister in the present work is designed with a quick plug in/pull out connector for easy replacement of a used (depletion) canister with a new (filled) one. The exchange process takes only about 1–2 min. The current gasoline stations or retail stores can serve a good network for selling and exchange of the hydrogen canisters [32]. In combination with the quick-replacement technique of the hydrogen canisters and the exchange model of hydrogen canisters, the driving range of the LEV can be largely extended.

2.4. Secondary battery

Lithium-ion batteries serve as supplemental power sources for propulsion of the LEV in the present work. They have a higher energy density than most other types of rechargeable batteries. This means that for their size or weight they can store more energy than other rechargeable batteries. In addition, lithium-ion batteries have a lower self-discharge rate than other types of rechargeable batteries. This means that once they are charged they will retain their charge for a longer time than other types of rechargeable batteries. Therefore, lithium-ion batteries are growing in popularity for electric vehicle applications.

The present lithium-ion battery module consists four 12 V, 40Ah packs connected in series, as shown in Fig. 8. The maximum power output from the lithium-ion battery was 2.7 kW. In combination of the maximum power delivered by the PEM fuel cell (6.0 kW), the hybrid power system could deliver the power up to 8.7 kW. Such power can reach the target performance of the LEV like the maximum speed and acceleration. In the present work, an integrated circuit component embedded in the microcontroller was designed to monitor the state of charge (SOC) for controlling charging and discharging current to protect the battery. The SOC of the lithium-ion battery is controlled between 30% and 80%, which will be discussed later.

2.5. Microcontroller

The operation of the hybrid power system requires a smart microcontroller together with the proper algorithm, which safely

Fig. 8. Photo of lithium-ion battery package.

starts, monitors and shuts down the hybrid power system under all operational conditions. The present work uses an Intel 8051 microprocessor as the head of the hybrid power system. The microcontroller is capable of monitoring the sensor signals of voltage, current, temperature, and pressure. It also takes proper actions to drive the external actuators such as the air blower, the solenoid valve, the water pump and the cooling fan. In addition, the voltage of each cell within the fuel cell stack is monitored in an analog multiplexer in order to detect individual cell failures early. Moreover, it monitors the SOC of the lithium-ion battery for controlling the charging/discharging current to protect the lithium battery from the overcharging/overdepletion. Most importantly, the microcontroller could allocate the best working voltages of the fuel cells in order to make the fuel cell generating power at the best efficient point. Furthermore, it hybridizes properly the fuel cell power and the battery power depending on the driving conditions. All operational parameters and data can be read directly from the display panel or can be downloaded to personal computer for further process through the RS232 communication port on the microcontroller.

2.6. DC–DC converter and other components

In general, the operational voltages for various power sources and external loads in the hybrid power system are different. For example, the nominal voltage of the present fuel cell stack is 48 VDC, while the operational voltage of the electrical motor of the LEV is 72 VDC. Therefore, it is necessary to boost and/or bulk the voltages of different power sources to ensure the DC-bus voltage on a stable level. In the present work, the DC/DC converter based on the PWM control schemes is used to transfer power among various power sources and loads. Besides the stabilization of the DC-bus voltage of the hybrid power system, the present DC/DC converter has the following important features. First, the DC/DC converter ensures the output voltage from the fuel cell stack higher than its cut-off voltage (40 VDC, Fig. 2) to avoid the damage of the fuel cell stack due to the concentration polarization. Then, it well regulates the charging current at different SOCs of the lithium-ion battery to prevent overcharge/overdepletion of the battery. Moreover, the DC/DC converter boosts the bus voltage to 72 VDC that requires for propelling the electrical motor and charging the lithium-ion battery. The efficiency of the DC/DC converter is higher than 92% at the operation power up to 2500 W.

Other components are either outsourcing or purchasing from the market (e.g., water pumps from IWAKI and air blowers from AMETEK). The details of these components can be assessed elsewhere, and are not elaborated on here due to the space limit.

3. System verification

3.1. Breadboard test

Fig. 9 shows the preliminary test of the hybrid power system on a breadboard for verify its availability. Basically, the breadboard test could help in the selection of components, the adjustment of system operating conditions, and the optimization of system layout. In addition, through the breadboard test, we could find out in advance whether the hybrid power system meets the performance targets or not. Hence, the hybrid power system can be optimized before installed on the light electric vehicle.

Before the breadboard test, each sensor is calibrated using a laboratory-quality instrument that ensures its accuracy (with uncertainties less than 5%) and reliability over the ranges in which it is operated. In the meantime, each actuator such as the solenoid valve and the relay is tested independently in order to check its availability and performance. These supported components are then installed on the hybrid power system spreading on the breadboard. The instrument for the breadboard test included data acquisition modules, voltage monitoring modules, electronic loads, and a personal computer along with the LabView-based graphic user interface (GUI). Important parameters of the hybrid power system, such as voltage, current, pressure, temperature, hydrogen flow rate, can be recorded. Meanwhile, load dynamics are simulated on the breadboard based on the real power requirement of the vehicle electrical motor.

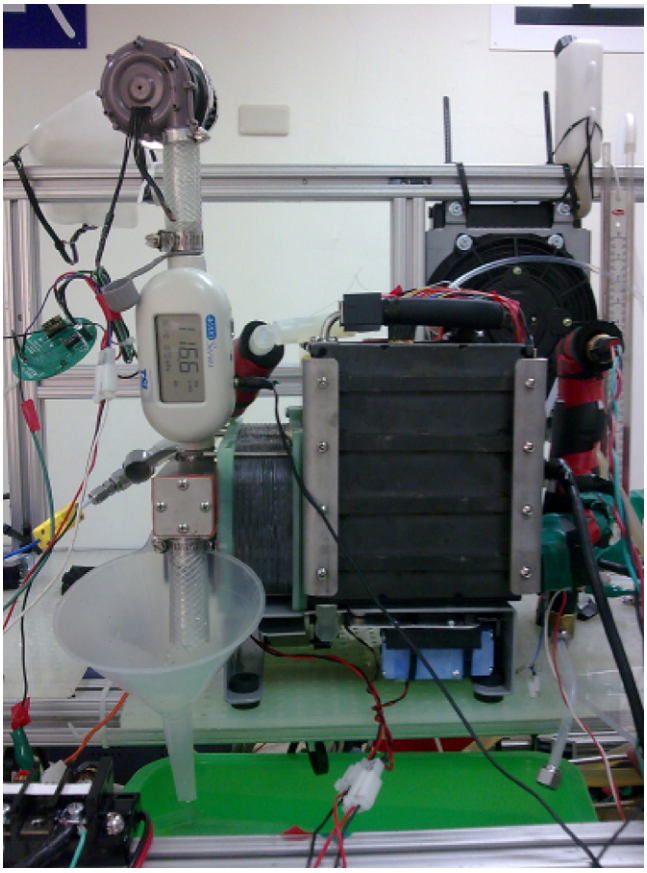

Fig. 9. Breadboard test of the hybrid power system.

3.2. System efficiency

The present hybrid vehicle is not capable in off-vehicle charge, which means that the battery cannot be charged from an off-vehicle electric energy sources. Therefore, the efficiency of the hybrid system should consider the power from the fuel cell alone. Intuitively, the efficiency of the hybrid power system could be determined by accounting for the generation efficiency of the fuel cell stack, the efficiency of the power conversion devices and the load of the power-consumed components. Table 3 lists the electric features of the auxiliary components in the hybrid power system. The present work, however, does not use such an approach since it is difficult to accurately determine the power consumption of the supported accessory and the efficiency of each power conversion device. For example, it is hard to catch the real power dissipation by the load-following blower, which fluctuates by the speed-up and the slow-down of the motor during the operation. The efficiency of the hybrid power system herein is defined as the ratio of the net

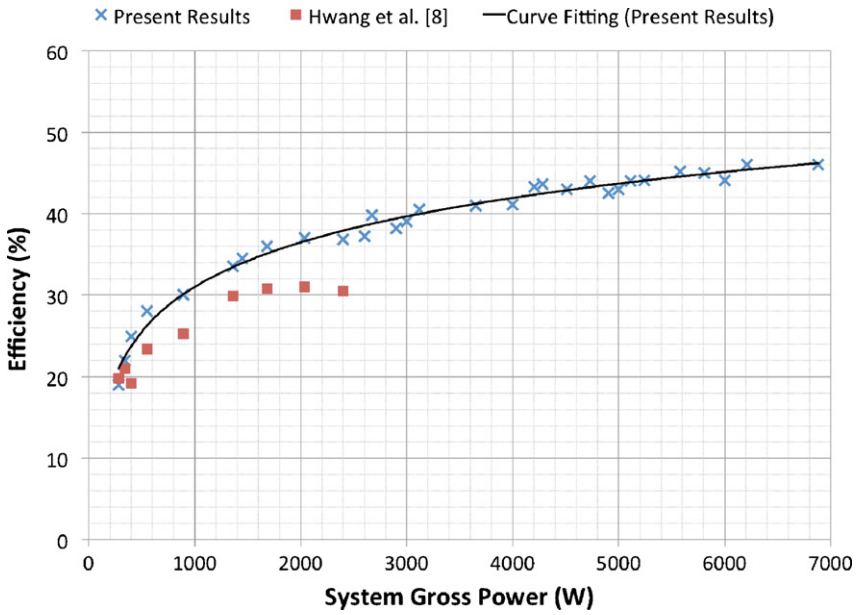

Fig. 10. Effect of gross power on the efficiency of the light electrical vehicle.

power requirement by the electric motor to the consumption of the hydrogen enthalpy, i.e.,

$$\varepsilon = \frac{I \times V \times \Delta t}{m \times \Delta h} \quad (1)$$

where V (V) is the voltage across the electric motor and I (A) is the current passing through the circuit. The amount of hydrogen consumption m (mol) is measured by subtracting the canister weight of discharged hydrogen from the refilled one in the test duration Δt (s).

Fig. 10 shows the system efficiency as a function of the gross power output of the hybrid power system. These data are based on static-load testing, which is a good representation of how the hybrid power system performs over a variety of loads. The cross symbols are the measured data while the curve is the fitting results from the data. The results of the prior generation of fuel cell LEV are included for comparison (solid squares) [8]. It is seen from this figure that the system efficiency is increased with increasing the gross power output, with the maximum efficiency up to 46%. In addition, the system efficiency of the present prototype is significantly higher than that of the prior one. This is because the present system used a new fuel cell stack of high performance. Moreover, the thermal-recycle design of using the stack waste heat to promote the dynamics of hydrogen desorption from the metal hydrides also helped enhancing the system efficiency.

Table 3
Typical power consumption/conversion efficiency of the components of the hybrid power system.

Components	Electric specification	Maximum power consumption/conversion efficiency
Air blower	24 V/10 A	250 W
Solenoid valve	12 V/0.12 A	2.8 W
Cooling fan	12 V/0.15 A	7.2 W
Water pump	24 V/0.8 A	20 W
Microcontroller	12 V/2 A	24 W
Converter I	48–72 VDC	92%
Converter II	48–12/24 VDC	92%

3.3. Road-drive test

The fuel cell/lithium-ion battery hybrid system is installed on the cargo of the LEV, as shown in Fig. 11. After installing the hybrid power system on the LEV and finishing the needed modifications, road-drive tests are conducted. The road-drive test of the LEV is done inside the campus of National University of Tainan, as shown in Fig. 12. Note that the safety of hydrogen vehicles is usually a matter of concern. Therefore, before each test run, regular leakage checks were conducted for the entire hydrogen feeding line such as the pipes, the fittings, the valves and the fuel cell stack. Once the microcontroller detects a parameter out of a prescribed range, it automatically performs a shutdown process. During the on-road test, several intermittent shutdowns were experienced due to the depletion of hydrogen and, fortunately, no accidents, hazardous or potentially hazardous situations occurred. In general, the road test has revealed that the LEV displays reliable operation without any failure for year driving. This indicates that the stability and reliability of the present system are, to a certain extent, satisfactory.

Fig. 11. Fuel cell/battery hybrid power system installed on the cargo of the light vehicle.

Fig. 12. Test drive of hybrid LEV in the campus of National University of Tainan.

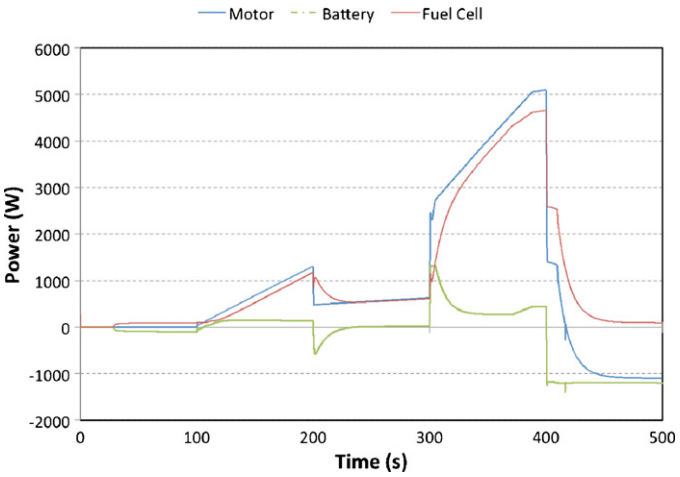

Fig. 14. Dynamics of hybrid power during the demonstration test.

3.4. Dynamics of the hybrid power system

Figs. 13 and 14 show the dynamics of the hybrid LEV under various driving conditions. Four typical driving modes, including idle, starting acceleration, slow driving, sharp acceleration, and braking, were tested to examine their dynamics.

Fig. 13 shows the variation of the vehicle speed during the test drive. The LEV is started up at time of 30 s and is kept standby (idle in speed) until 100 s. It was accelerated from 0 to 22 km-h^{-1} during 100–200 s, and then increases its speed with a slower acceleration to 28 km-h^{-1} at 300 s. Moreover, the LHV was accelerated to 58 km-h^{-1} at 400 s. Finally, the driver braked the LEV to decelerate the LEV to 50 km-h^{-1} at 500 s.

By observing the recording data of the hybrid power system, the dynamics of the vehicle was illustrated as follows. The hybrid power system of the LEV was turned on at time of 30 s and the LEV remained idle before 100 s. During this period of 30–100 s, the motor did not consume any power, and the fuel cell charged the lithium-ion battery. At the time of 100 s, the driver started pressing the accelerating pedal of the LEV. The power delivered by the lithium-ion battery quick responded to that required by the motor. The fuel cell then increased its power to meet the trend of the power demand of the electric motor.

At the time of 200 s, the driver slightly released the pedal of the LEV, thus reducing the acceleration of the LEV. In this circumstance, the power demand by the electric motor dropped down from 1.3 kW to 0.5 kW. Because the response of the fuel cell was slow, the excess power from the fuel cell was used to charge the lithium-ion battery. After 240 s, the fuel cell power met that of the motor. Therefore, the above charge status ceased. From 240 s to 300 s, the power demand of the electric motor was relatively stable and thus the fuel cell could power the electric motor totally.

At the time of 300 s, the acceleration of the LEV increased, and thus the power required by the electric motor increased dramatically again. At this point, the response of the fuel cell could not catch up the power dynamics of the motor. Therefore, a large portion of the motor power should be delivered from the lithium-ion battery. When the power delivered by the fuel cell increased gradually, the power extracted from the lithium-ion battery was therefore decreased. During the period 300 s–400 s, the fuel cell power could not satisfy the power demand of the electric motor alone. The power demands of the LEV were dependent not only on the fuel cell but also on the lithium-ion battery. The lithium-ion battery started to provide power to the electric motor as a back up.

From time of 400 s, the driver braked the LEV with a linear deceleration. Since the nature of slow dynamics of fuel cells, the power delivered by the fuel cell should decreased gradually over the response time. The excess power was therefore charged into the lithium-ion battery. However, the power absorbed by the lithium-ion battery was limited by the charge capacity (current). The extra

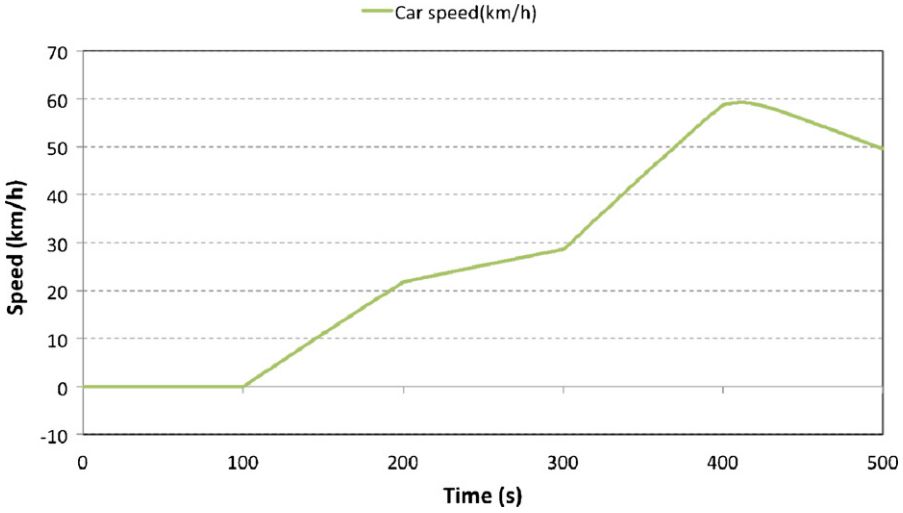

Fig. 13. Variation of speed of the LEV during the demonstration test.

power that the lithium-ion battery could not absorb was provided to the electric motor, such that the electric motor maintained its power at about 1.3 kW for seconds before decreasing power. From time of 460 s, the motor power became negative, meaning that the motor entered the regenerative mode, which transformed the kinetic energy into the electrical one. In this circumstance, both the fuel cell power and the regenerative power from the motor were stored in the lithium-ion battery.

4. Conclusions

In the present work, a hybrid power combining a lithium-ion battery and a PEM fuel cell has successfully propelled a light electric vehicle. These two power sources are connected in parallel. In general, the lithium-ion battery supplies power to compensate for the deficiencies of the fuel cell, while storing extra power provided by the fuel cell and regenerative braking. Original results from the present work are summarized as follows.The present work has successfully integrated the fuel cell stack and the membrane humidifier into a compact unit that has the advantages in the reduction of components and space saving.The present system has thermally coupled the fuel cell stack and the metal hydride storage. During the electrification, the thermal wastes from the fuel cell stack have been recycled to the metal hydrides to supply the heat for desorption of hydrogen.The efficiency of the hybrid power system is increased with increasing gross power output, with the maximum efficiency up to 46%. As compared to the previous prototype, the present system has a higher efficiency. This is because of the use of the new generation of fuel cell stack and, partly, the design of recycling the stack thermal wastes to help hydrogen desorption from the metal hydrides.

Acknowledgments

The author Jenn Jiang Hwang would like to thank the National Science Council of Taiwan, for financially supporting this research under Contract no 982A33. Technical supports by Asia Pacific Fuel Cell Technologies (Taiwan) are also appreciated.

References

[1] J.J. Hwang, Renew. Sust. Energy Rev. 15 (2011) 1392.
[2] P. Corbo, F. Migliardini, O. Veneri, Renew. Energy 34 (2009) 1955.
[3] M. Granovskii, I. Dincer, M.A. Rosen, Int. J. Hydrogen Energy 31 (2006) 337.
[4] Rainforests, R.I.C. Publications, 2005, ISBN 9781741263305.
[5] Green Vehicle Guide, Green Student U., http://www.greenstudentu.com/encyclopedia/green_vehicle_guide, Retrieved 2011-12-29.
[6] Alternative and Advanced Vehicles, Alternative Fuels and Advanced Vehicle Data Center, U.S. Department of Energy, http://www.afdc.energy.gov/afdc/vehicles/index.html, retrieved 2011-12-29.
[7] S. Daniel, D. Gordon, Two Billion Cars: Driving Toward Sustainability, Oxford University Press, New York, 2009, ISBN 978-0-19-537664-7.
[8] J.J. Hwang, D.Y. Wang, N.C Shih, J. Power Sources 141 (2005) 108.
[9] R.M. Moore, K.H. Hauer, S. Ramaswamy, J.M. Cunningham, J. Power Sources 159 (2006) 1214.
[10] K. Jorgensen, Utilities Policy 16 (2008) 72.
[11] C.E. Thomas, Int. J. Hydrogen Energy 34 (2009) 6005.
[12] D.D. Boettner, M.J. Moran, Energy 29 (2004) 2317.
[13] Y. Swesi, D. Ronze, I. Pitault, R. Dittmeyer, F. Heurtaux, Int. J. Hydrogen Energy 32 (2007) 5059.
[14] A. Dalvi, M. Guay, Control Eng. Pract. 17 (2009) 924.
[15] E. Schiebwohl, T. Unwerth, F. Seyfired, J. Power Sources 193 (2009) 107.
[16] W.R. Chang, J.J. Hwang, J. Power Sources 166 (2007) 149.
[17] J.J. Hwang, C.H. Chao, J. Chin. Mech. Eng. 24 (2007) 367.
[18] J.J. Hwang, C.K. Chen, R.F. Savinell, C.C. Liu, J. Wainright, J. Appl. Electrochem. 34 (2004) 217.
[19] R.M. Moore, K.H. Hauer, D. Friedman, J. Power Sources 141 (2005) 272.
[20] J.J. Hwang, S.D. Wu, L.K. Lai, J. Power Sources 161 (2006) 240.
[21] J.J. Hwang, J. Electrochem. Soc. 153 (2006) A216.
[22] J.J. Hwang, C.H. Chao, Int. J. Hydrogen Energy 32 (2007) 405.
[23] J.J. Hwang, J. Chin. Mech. Eng. 29 (2008) 195.
[24] Al-Baghdadi Maher A.R. Sadiq, Renewable Energy 34 (2009) 674.
[25] J. Wu, X.Z. Yuan, M.J. Jonathan, H. Wang, D. Yang, J. Qiao, J. Power Sources 195 (2010) 1171.
[26] J.J. Hwang, W.R. Chang, A. Su, Int. J. Hydrogen Energy 33 (2008) 3801.
[27] T. Sakai, I. Uehara, H.J. Ishikawa, Alloys Compd. 762 (1999) 293.
[28] J.J. Hwang, T.M. Liou, Int J. Heat Mass Transfer 38 (1995) 3197.
[29] Y.S. Yang, M. Kao, 2004, US patent 6742650.
[30] Z. Jiang, R.A. Dougal, S. Liu, S.A. Gadre, A.D. Ebner, J.A. Ritter, J. Power Sources 142 (2005) 92.
[31] Y.S. Yang, Y.S. Hsu, 2005, US patent 6857396.
[32] J.J. Hwang, W.R. Chang, Int. J. Hydrogen Energy 35 (2010) 11947.